

# GIS based statistical and physical approaches to landslide susceptibility mapping (Sebinkarahisar, Turkey)

Işık Yılmaz · Inan Keskin

Received: 25 February 2008 / Accepted: 5 November 2008 / Published online: 27 January 2009  
© Springer-Verlag 2009

**Abstract** The case study presents GIS-aided statistically and physically based landslide susceptibility mapping in the landslide-prone Avutmus district of Sebinkarahisar (Giresun, Turkey). Field investigations, analysis of geological data and laboratory tests suggested that two important factors have acted together to cause sliding: ground water pressures and toe erosion. Frequency ratio (FR) and stability index mapping (SINMAP) were used to create the landslide susceptibility maps based on a landslide inventory; distance from drainage systems, faults and roads; slope angle and aspect; topographic elevation and topographical wetness index; and vegetation cover. Validation of the models indicated high quality susceptibility maps with the more realistic results were obtained from the statistically based FR model.

**Keywords** Toe erosion · Sebinkarahisar (Giresun, Turkey) · Landslide · Susceptibility map · GIS · Frequency ratio · SINMAP

**Résumé** L'étude de cas présente une cartographie de sensibilité aux glissements de terrain basée sur une approche physique et statistique, avec le support d'un SIG, cartographie réalisée dans le district d'Avutmus sujet aux glissements, région de Sebinkarahisar (Giresun, Turquie). Les travaux de terrain, les analyses de données géologiques et les essais de laboratoire ont fait apparaître deux facteurs importants agissant conjointement, à l'origine des glissements: les pressions d'eau du sol et l'érosion de pied de versant. Les indices FR (fréquence des événements) et

SINMAP (indice de stabilité) ont été utilisés pour réaliser les cartes de sensibilité aux glissements, prenant appui sur un inventaire des glissements, la distance aux axes de drainage, aux failles et aux routes, la pente et la morphologie des terrains, la position topographique, l'indice d'humidité, la couverture végétale. La validation des modèles permet de souligner la qualité de ces cartes de sensibilité, les résultats les plus réalistes étant obtenus à partir du modèle des fréquences d'événements qui s'appuie sur une approche statistique.

**Mots clés** Erosion de pied de versant · Sebinkarahisar (Giresun, Turquie) · Glissement de terrain · Carte de sensibilité · SIG · Fréquence d'événements · SINMAP

## Introduction

Landslides are frequently responsible for considerable loss of money and lives. Landslides and related slope stability problems disturb many parts of the world but experience indicates that understanding, recognition and treatment of landslide hazards is still fragmentary. A particular area requiring attention concerns the selection and design of appropriate, cost-effective remedial measures, which in turn require a clear understanding of the conditions and processes that caused the landslides. Much progress has been made in developing techniques to minimize the impact of landslides, although more efficient, quicker and cheaper methods could well emerge in the future. Landslides may be corrected or controlled by one or more combinations of four principle measures: drainage, slope geometry modification, retaining structures and internal slope reinforcement.

I. Yılmaz (✉) · I. Keskin  
Faculty of Engineering, Department of Geology,  
Cumhuriyet University, 58140 Sivas, Turkey  
e-mail: iyilmaz@cumhuriyet.edu.tr

As stated by Ercanoglu and Gokceoglu (2004), production of landslide susceptibility maps at the early stage has a crucial importance for safe and economic planning of urban development and engineering structures. However, a standard procedure for the production of landslide susceptibility maps does not exist. For this reason, many researchers have used different techniques such as the heuristic approach (Ives and Messerli 1981; Rupke et al. 1988; Barredo et al. 2000; Van Westen et al. 2000; Van Westen and Lulie Getahun 2003), deterministic models (Ward et al. 1982; Cascini et al. 1991; Gokceoglu and Aksoy 1996), statistical methods (Van Westen 1993; Chacón et al. 1994, 1996; Chung and Fabbri 1999; Dai et al. 2001; Lee and Min 2001; Carrara et al. 2003; Yilmaz and Yildirim 2006) and parameters to evaluate landslide susceptibility in different parts of the world. Because of the deficiencies in understanding pore water pressure development in soils, including their spatial and temporal distribution, some physical models have been developed. Well-known physically based approaches for assessing slope stability and hazards have been developed by Hammond et al. (1992), Montgomery and Dietrich (1994) and Pack et al. (1998a, b). Borga et al. (1997) applied the physically based model proposed by Montgomery and Dietrich (1994) in the eastern Italian Alps (Cordon Basin) and reported that most of the scars were correctly identified, although many more cells were predicted to be unstable than observed. Calcaterra et al. (2004) created the susceptibility index (SI) map with a SINMAP model for a shallow landslide area in the Agnano plain in Naples (Italy) and found that only one of the 49 slides fell in the regions characterized by the lowest SI. Chacón et al. (2006) also reported some successful applications of physically based models for producing landslide susceptibility maps.

In this paper the mechanism of the landslides south of Giresun, Turkey, is described and some remedial solutions proposed. In order to select probable landslides for risk-management studies, landslide susceptibility maps of the study region and surrounding areas were prepared using GIS-aided statistical frequency ratio (FR) and physical (SINMAP) models. Finally, the landslide susceptibility maps obtained from the two different models are compared and discussed.

## Study area

### Geographical setting

The location of the study area at Sebinkarahisar, Turkey is shown in Fig. 1a. The main drainage system is dominated by the Avutmus creek which extends SW–NE. The 1:25,000 scale digital elevation model (DEM) of the study

area indicated topographical elevations ranging from 950 to 1,400 m and average slope angles of 20°, rising to 84° in some locations.

Rainfall is the main source of water in the study area, which receives an average annual rainfall of 590 mm. Most of the rainfall occurs during April, with a mean value of 86.6 mm. Meteorological records of 20 years (1985–2004) showed that the annual average maximum temperature is 20°C in August whereas the annual average minimum temperature (always recorded in January) is −2.1°C (Table 1).

On a number of occasions, the material forming moderately steep slopes failed at times of heavy rainfall and affected homes, farm buildings, etc. (Fig. 2). A long history of ground movements together with river erosion at the toe and a change in the groundwater regime within the slope created the pre-conditions for landsliding. Site investigations characterized the ground conditions and identified the active slip surface within the compound landslide terrain.

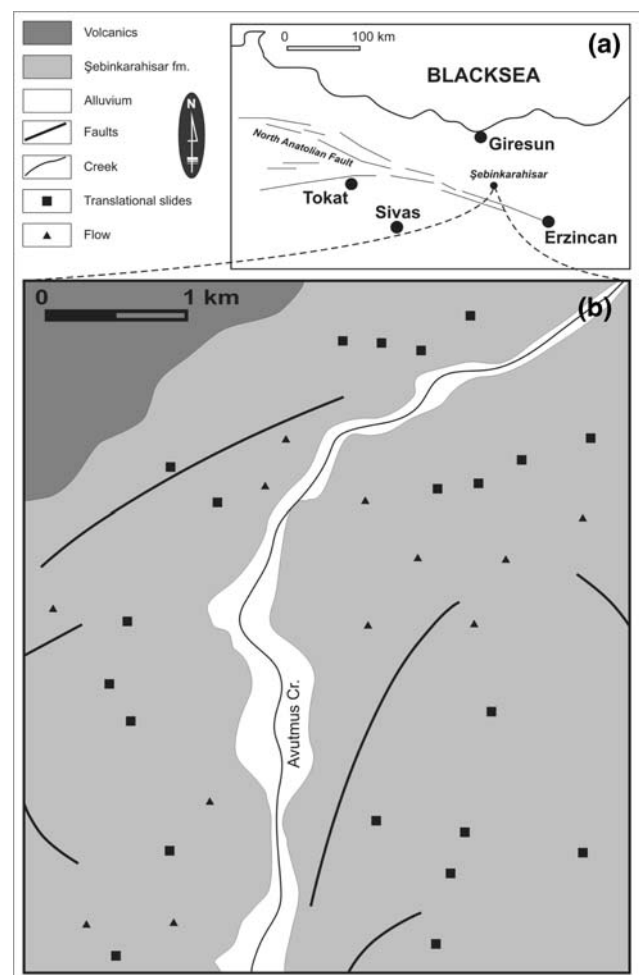


**Fig. 1** Location and simplified geological map of the study area

**Table 1** Annual rainfall and temperature in Sebinkarahisar (1985–2004)

	Jan.	Feb.	Mar.	Apr.	May.	June	July	Aug.	Sep.	Oct.	Nov.	Dec.	Annual
Rainfall (mm)	51.1	51.8	51.5	86.6	75.1	45.9	12.3	7.4	24.3	58.6	68.2	57.2	590
Temperature (°C)	−2.1	−1.6	2.3	9.0	12.9	16.3	19.8	20.0	16	11	4.2	−0.1	9

**Fig. 2** **a** A view from landslides, and **b** bridge destroyed by Avutmus creek

### Stratigraphic and tectonic settings

The study area encompasses three units ranging in age from Eocene to Quaternary. The Eocene volcanics are the oldest, overlain by the Sebinkarahisar Formation of Oligo-Miocene age with Quaternary alluvium accumulating within the river valley (Fig. 1b).

Weathered, crushed and jointed, grey/black andesites and basalts have sparse outcrops in the study area (Yilmaz et al. 1985). The Oligo-Miocene Sebinkarahisar Formation consists of red fissured clay and claystone, uncemented loose sandstone and conglomerates, with gypsum found in some locations. This Formation is the most extensive surface geology in the study area, unconformably overlying

the volcanics. Indeed, the lower part of the Sebinkarahisar Formation consists of red clays derived from weathering of the andesite–basalt. The alluvium consists of stratified materials of heterogeneous grain sizes, derived from various geological units in the vicinity.

Turkey is characterized by major intercontinental strike-slip faults—the dextral North Anatolian Fault Zone and the sinistral East Anatolian Fault Zone. Between these the Anatolian block moves westward relative to the Eurasian plate in the north and the Arabian plate in the south, as a consequence of the continued convergence of these plates since the middle Miocene (McKenzie 1972; Dewey and Şengör 1979; Şengör 1980; Barka and Gülen 1988; Koçyiğit 1989); see Fig. 3.

As seen in Fig. 3, other secondary faults are the left-lateral Central Anatolian Fault Zone (CAFZ), the right-lateral Salt Lake Fault Zone (SLFZ) and the İnönü-Eskişehir and Akşehir oblique-slip normal fault zones (Koçyiğit and Özacar 2003).

### Description and mechanism of the landslide

The study area is frequently subjected to landslides (Fig. 2). Geological and geotechnical studies were conducted on one of the landslides to gain a better understanding of the triggering mechanisms and failure process and to better prepare for future failures in the area. The velocity of the slope movement has been predicted by monitoring the relative building movements over 2 years. Following Varnes (1978), the rate of movement would be classified as slow (i.e., 0.06–1.5 m/month) but very high rates were recorded after heavy rain increased the water level in the rivers and hence their erosive power.

Soil mechanics tests, in accordance with American Standards Testing of Materials (ASTM 1990), were carried out on 30 samples collected from the landslide material. The particle size analyses indicated the basalt-derived soils had 4% gravel, 29% sand, 38% silt and 29% clay-sized material (Fig. 4a). Most of the samples tested were of low plasticity, with liquid limits ranging between 27 and 54% (average 40%). The plasticity index extended from 10 to 26%, averaging 17%, whereas the average plastic limit value was 23% (range 17–32%). As seen in Fig. 4b, when plotted on the plasticity chart 17% of the samples classified as CH (high plasticity, inorganic clay); these samples were generally taken from the depth close to the sliding surface.

**Fig. 3** Tectonic map of Turkey (after Koçyigit and Özacar 2003)

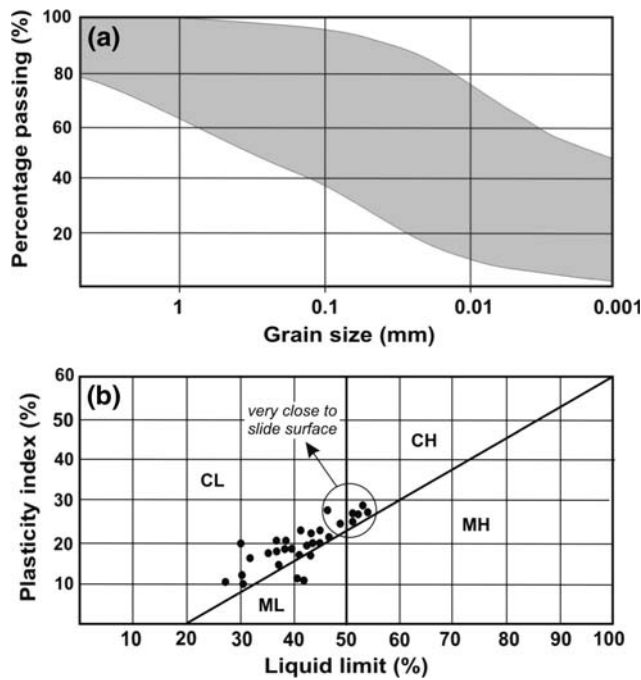
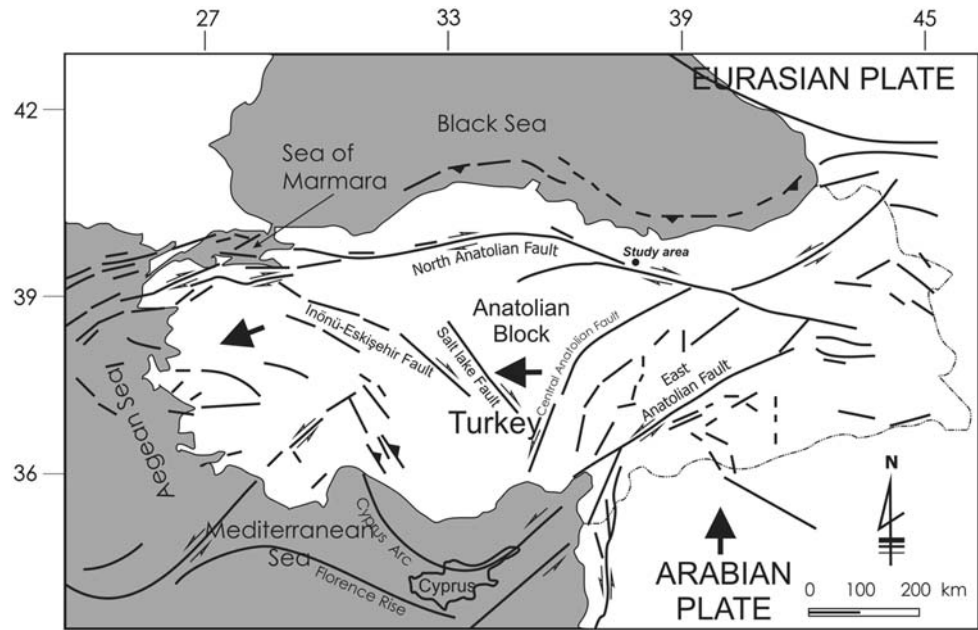


**Fig. 4** a Grainsize distribution, b soil classification of landslide-forming material

Low plasticity, inorganic clays (CL) account for 73% of the samples while 10% were ML (low plasticity, inorganic silt). Such soils are prone to flow when the moisture content is as low as 50% and when present between the surface veneer and the basement rock will contribute to a susceptibility to slope movement.

The geotechnical characteristics of soils are associated with their mineralogical composition, especially with their

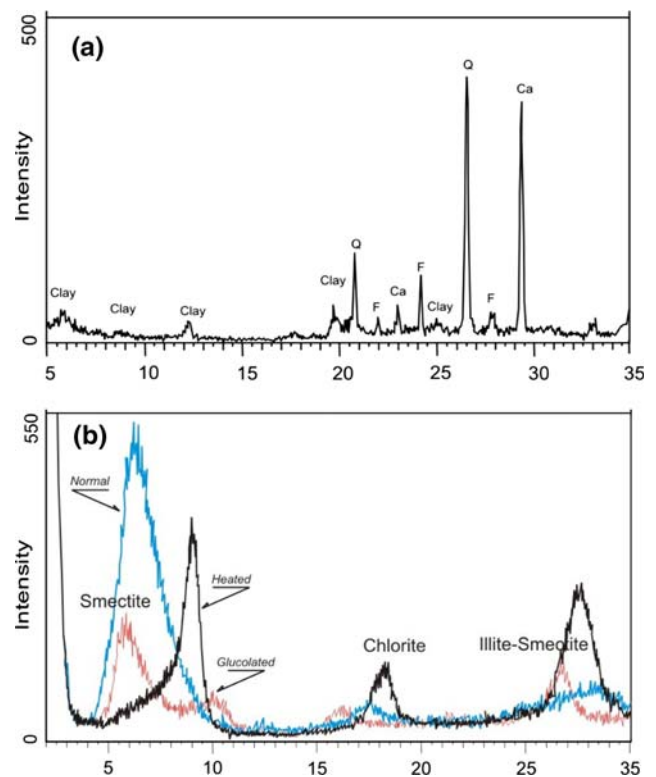


**Fig. 5** Characteristic X-ray diffraction diagrams of whole-rock powder (a) and oriented samples (b)

clay mineralogy hence the mineralogy of the 30 samples was determined by whole-rock powder X-ray diffraction and oriented samples of the clay-size fraction. As seen in Fig. 5a and Table 2, the results indicated the soils were



**Table 2** Semi-quantitative results of X-ray diffraction determination

Minerals (%)	Minimum	Maximum	Mean value
Clay	45	73	55.4
Calcite	2	35	15.8
Quartz	10	28	16.5
Feldspar	1	16	7.5
Clay minerals			
Smectite	55	100	80
Illite–smectite	15	23	15
Chlorite	2	10	5

composed of clay, calcite, feldspar and quartz minerals. More than half the material is indicated as clay, with smectite being the dominant clay mineral.

Standard penetration tests (SPTs) were undertaken in boreholes drilled at three locations. The  $N$  values ranged from 17 to 38, average 22. The internal friction angle and cohesion were assessed from laboratory and SPT tests; values of  $5^{\circ}$ – $40^{\circ}$  and 0–35 kPa. This large variation is indicative of the lateral and vertical inhomogeneity of the slope-forming materials.

The landslides usually occur on the slopes above the Avutmus creek, which has a very high velocity and discharge in winter, suggesting that undercutting of slopes by surface water is the primary cause; i.e., a combination of the removal of lateral support and increased loading as a consequence of rising groundwater level is thought to be the triggering mechanism hence the slope stability is in part related to distance from the river. The landslide mechanism is shown in Fig. 6. The deep-seated elements of the landslide involve translational sliding on the red clay above the volcanic rocks. As seen in the figure, the scars upslope indicate regressive failure. As each cell of the slide moves forward, there is a reduction of the loading of the clay layer, resulting in some dilation, uptake of water and hence loss of strength.

In addition to sliding, where loose, weak rocks are present on a steep slope, the loading created by intense rain causes the material to effectively flow downslope.

### Landslide susceptibility mapping

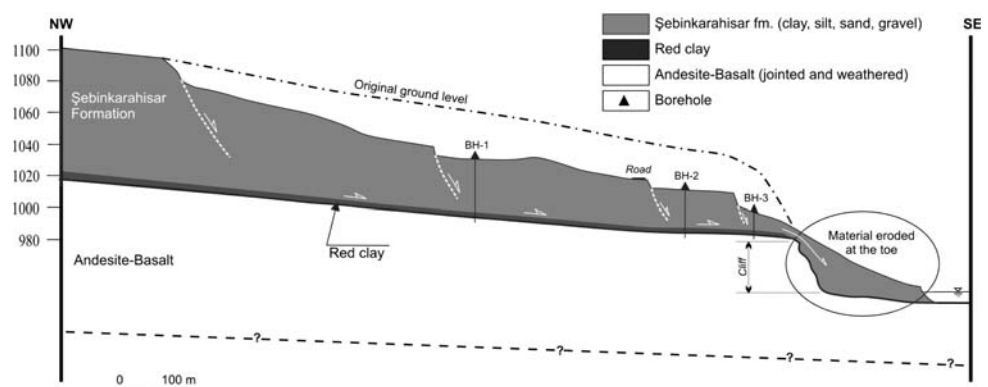
In recent years, technologies have been developed which present possibilities for a wide range of disaster management and hazard mitigation methods. Several attempts have been made to understand the temporal–spatial distribution of landslides and thus minimize possible impacts by means of predictive risk models. Quantitative techniques have become very popular in the last decades as a consequence of developments in computer and GIS technology.

To predict landslide locations, it is generally assumed that landslide occurrence is determined by particular factors and that past and future landslides occur under similar circumstances (Lee and Talib 2005). In order to construct the landslide susceptibility map quantitatively, the FR model was used by means of GIS as shown in the flowchart (Fig. 7). FR is the ratio of the area where landslides occurred to the total study area, and the ratio of the probability of a landslide occurrence to a non-occurrence for a given attribute (Eq. 1) (Bonham-Carter 1994; Lee and Talib 2005).

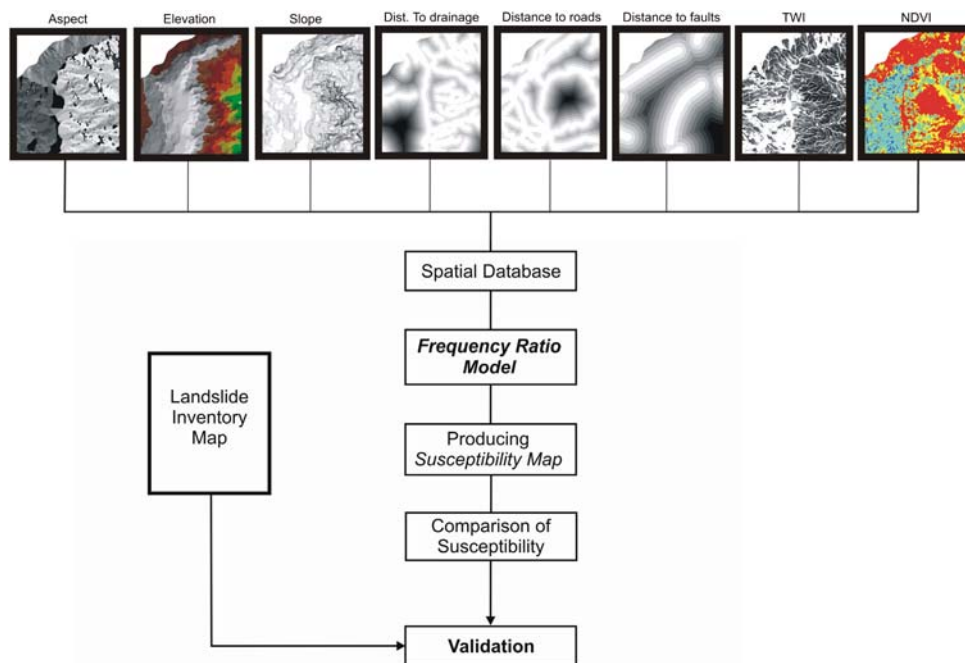
$$FR = (\text{LOG}/\text{TLOG})/(\text{GD}/\text{TGN}) \quad (1)$$

where FR, frequency ratio of each factor's type or range; LOG, number of landslide occurrence grids in factor's range or type; TLOG, number of landslide occurrence grids in study area; G, grids in factor's range or type; TGN, number of total grids in study area.

The use of models for predicting hydrological processes and slope stability is increasingly common at the catchment scale. Many models operate within GIS frameworks, using DEMs created from digital elevation data that are readily available through various sources. Output from models can assist specialists in delineating areas of potential instability and provide an objective, quantitative analysis of terrain

**Fig. 6** Cross-section showing the landslide mechanism

**Fig. 7** The procedure of landslide susceptibility assessment based on frequency ratio model



stability to complement the qualitative field and office-based assessments.

Much research has focused on understanding and measuring the physical factors controlling stability, in conjunction with developing tools and techniques to predict landslide occurrences. *SINMAP* is an ArcView extension that calculates and maps a slope stability index, based on geographical information and geotechnical data. The model is a slope stability predictive tool which includes a hydrologic flow modeling component. It uses the surface topography to route flow down-slope, assuming that the subsurface hydrologic boundary parallels the surface, and soil thickness and hydraulic conductivity are uniform. The flow model predicts relative levels of groundwater across a watershed area. This prediction is then used to assess slope stability.

#### Frequency ratio model

The study area has experienced many landslides over a long period; 33 landslides (21 rotational and 12 flows) have been mapped (Fig. 1b). In order to prepare an inventory map, landslide locations were plotted on a 1:25,000 scale topographic map using the Landsat TM satellite images and 1:35,000 aerial photographs. This information was completed and confirmed by the field surveys (Fig. 8).

Geological, morphological, hydrogeological and meteorological conditions, vegetation and land use are among the factors which influence the occurrence of landslides. The intensity of precipitation was ignored in this study, as it is very similar throughout the area and hence its effect

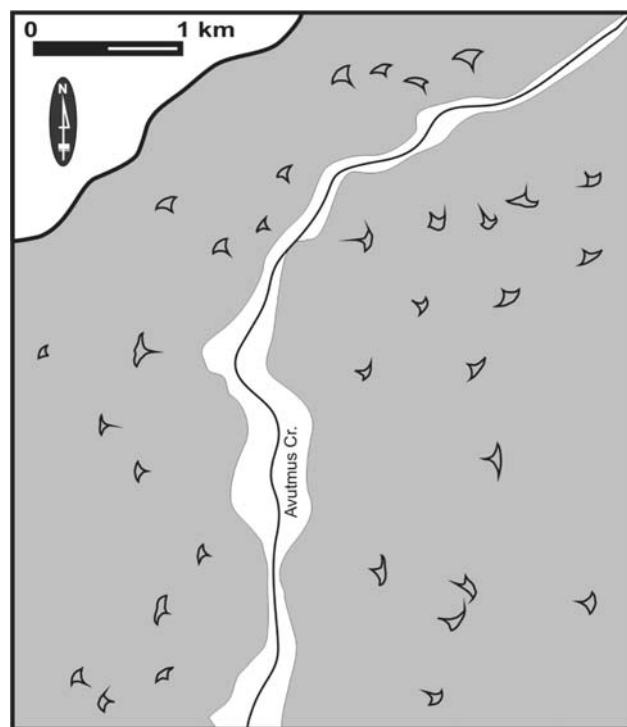


**Fig. 8** Landslide inventory map

was considered effectively consistent. ArcGIS 9.1 (2005) was used as a basic tool for spatial management and data manipulation.

First the FR was calculated for each range or type of factor, then the FRs were summed to calculate the landslide susceptibility index (LSI) following Lee and Talib (2005).

$$LSI = \sum FR \quad (2)$$

Parameter maps of geology, topography and environment were used in the susceptibility analyses. The cell size selected for the landslide and parameter maps was  $10 \times 10$  m as the working scale was 1:25,000. These maps consist of 500 rows and 455 columns, i.e., 227,500 cells.

### Geological parameters

There are three types of geological units in the study area. As seen in Fig. 1b, the largest is the Sebinkarahisar Formation. The volcanics found in the northwest of the study area were eliminated as all the known landslides have occurred in the Sebinkarahisar Formation. Lineaments in the study area were determined based on field observations, the 1:35,000 scale aerial photographs and satellite images. They are generally strike-slip with a SW–NE trend. Distance to faults was calculated at 150 m intervals by buffering. As seen in Table 3, FR increases closer to the faults.

### Topographical parameters

Topographical elevation, slope angle, slope aspect and topographic wetness index (TWI) and drainage system data were obtained from the DEM constructed using ArcGIS 9.1 (2005). Distances between landslides and surface drainage were calculated at 100 m intervals. As seen from Table 3, closer to the drainage system, FR values greater than 1 were obtained indicating a high probability of landslide occurrence, consistent with toe erosion as a major cause of failure. In the analysis, a transmissivity value of 1 was used for the whole catchment area.

Topography affects the spatial distribution of soil moisture with groundwater movement often following the surface topography (Burt and Butcher 1986; Seibert et al. 1997; Rodhe and Seibert 1999; Zinko et al. 2005) hence topographic indices were used to describe the spatial soil moisture patterns (Burt and Butcher 1986; Moore et al. 1991). One such index is the TWI developed by Beven and Kirkby (1979) within the runoff model. It is defined as:

$$TWI = \ln(a / \tan \beta) \quad (3)$$

where  $a$  is the local upslope area draining through a certain point per unit contour length and  $\tan \beta$  is the local slope. Although higher TWI values were found at higher elevations (Fig. 9), these result from rainfall infiltrating into the slope-forming materials. However, due to the topographic slope, the water moves through the near-surface materials to create higher pore pressures where the slope elevation is lower; it was observed that landslides are more abundant at

the lower elevations (1,000–1,200 m). In addition, steeper slopes are generally less susceptible to shallow landslides due to the outcrop of bedrock or the high permeability/transmissivity of any surface talus.

The slopes in the study area are oriented towards the creek, which in the northern part extends NE–SW (Fig. 1). FR analyses showed landslides occur dominantly where the slope angle is between  $10^\circ$  and  $35^\circ$ .

### Environmental parameters

Vegetation cover and closeness to roads were considered. The normalized difference vegetation index (NDVI) is a measure of surface reflectance and gives a quantitative estimate of the vegetation growth and biomass (Hall et al. 1995). Very low values of NDVI (0.1 and below) correspond to barren areas, sand or snow. Moderate values (0.2–0.3), represent shrub and grassland while high values (0.6–0.8) indicate temperate and tropical rainforests (Weier and Herring 2005). The NDVI was calculated from the following formula.

$$NDVI = (IR - R) / (IR + R) \quad (4)$$

where

IR infrared portion of the electromagnetic spectrum  
R red portion of the electromagnetic spectrum

The relationship between landslide occurrence and NDVI can be seen in Table 3, which indicates a positive correlation between landslide occurrence and NDVI. It was observed that the landslides occurred mainly in grassland and forested areas, with NDVI values of 0.1–0.3 and 0.6–0.84, respectively.

Table 3 also indicates that proximity to roads increases the probability of landslide occurrence, due to cuttings on the upslope side and increased loading/embankments on the downslope side.

### Construction of susceptibility map and validation of the model

The susceptibility map (Fig. 10) was constructed using the equal area method and five categories were determined. As suggested by Yilmaz (2007), a non-hierarchical cluster analysis was used to define the five groups as objectively as possible. Higher LSI values indicate the combination of factors is more likely to result in landsliding.

The susceptibility map was validated by field studies. Only three landslides in the study area were located in the unstable zone on the susceptibility map. As a result of control for FR model, 90% of the landslide occurrence

**Table 3** Frequency ratio of factors in landslide occurrence

	LSOG (%)	Grid (%)	FR		LSOG (%)	Grid (%)	FR
DFD (m)				Slope aspect			
0–100	0.41	0.37	1.11	Flat	0.04	0.08	0.46
101–200	0.26	0.20	1.28	N	0.04	0.04	1.04
201–300	0.13	0.11	1.13	NE	0.08	0.07	1.11
301–400	0.08	0.07	1.10	E	0.14	0.13	1.11
401–500	0.06	0.06	1.09	SE	0.16	0.15	1.06
501–600	0.03	0.04	0.70	S	0.11	0.13	0.82
601–700	0.02	0.04	0.39	SW	0.10	0.11	0.97
701–800	0.02	0.04	0.45	W	0.13	0.12	1.13
801–900	0.00	0.03	0.10	NW	0.16	0.14	1.14
>900	0.00	0.04	0.00	N	0.05	0.04	1.11
DFD (m)				Elevation (m)			
0–150	0.10	0.09	1.14	940–1,000	0.06	0.17	0.34
151–300	0.16	0.10	1.51	1,001–1,050	0.30	0.21	1.40
301–450	0.19	0.15	1.28	1,051–1,100	0.33	0.22	1.49
451–600	0.16	0.14	1.20	1,101–1,150	0.20	0.15	1.33
601–750	0.16	0.13	1.19	1,151–1,200	0.10	0.09	1.20
751–900	0.14	0.13	1.08	1,201–1,250	0.01	0.06	0.17
901–1,050	0.05	0.08	0.64	1,251–1,300	0.00	0.05	0.00
1,051–1,200	0.03	0.05	0.50	1,301–1,350	0.00	0.03	0.00
1,201–1,350	0.01	0.05	0.20	1,351–1,400	0.00	0.01	0.00
>1,350	0.00	0.08	0.05	>1,400	0.00	0.00	0.00
Slope angle				TWI			
0–5°	0.17	0.18	0.91	1.55–3.31	0.11	0.15	0.77
6–10°	0.24	0.26	0.92	3.31–5.08	0.16	0.17	0.93
11–15°	0.23	0.20	1.17	5.08–6.85	0.19	0.18	1.07
16–20°	0.15	0.11	1.38	6.85–8.62	0.15	0.15	1.01
21–25°	0.10	0.07	1.34	8.62–10.39	0.13	0.12	1.09
26–30°	0.07	0.05	1.26	10.39–12.16	0.07	0.08	0.88
31–35°	0.04	0.03	1.09	12.16–13.93	0.05	0.05	1.05
36–40°	0.01	0.03	0.25	13.93–15.70	0.04	0.04	1.09
41–45°	0.00	0.03	0.06	15.70–17.47	0.05	0.04	1.36
46–79°	0.00	0.03	0.00	17.47–19.19	0.03	0.02	1.48
NDVI				DFR (m)			
–0.9–0.1	0.39	0.44	0.89	0–100	0.40	0.37	1.10
0.1–0.3	0.21	0.13	1.58	101–200	0.30	0.23	1.27
0.3–0.6	0.27	0.36	0.74	201–300	0.16	0.14	1.20
0.6–0.84	0.13	0.07	2.05	301–400	0.05	0.07	0.62
				401–500	0.02	0.05	0.47
				501–600	0.01	0.03	0.42
				601–700	0.01	0.02	0.37
				701–800	0.02	0.03	0.71
				801–900	0.01	0.02	0.61
				>900	0.01	0.02	0.29

LSOG landslide occurrence grids, FR frequency ratio, DFD distance from drainage, DFF distance from faults, DFR distance from roads

locations fell into the susceptible classes. Figure 11 illustrates the distribution of landslides within the susceptibility classes. Validation of the map indicated the high quality of the results obtained in this study.

#### Physically based susceptibility mapping

As many shallow seated rotational slides were observed in the study area, an evaluation of the Stability *IN*dex



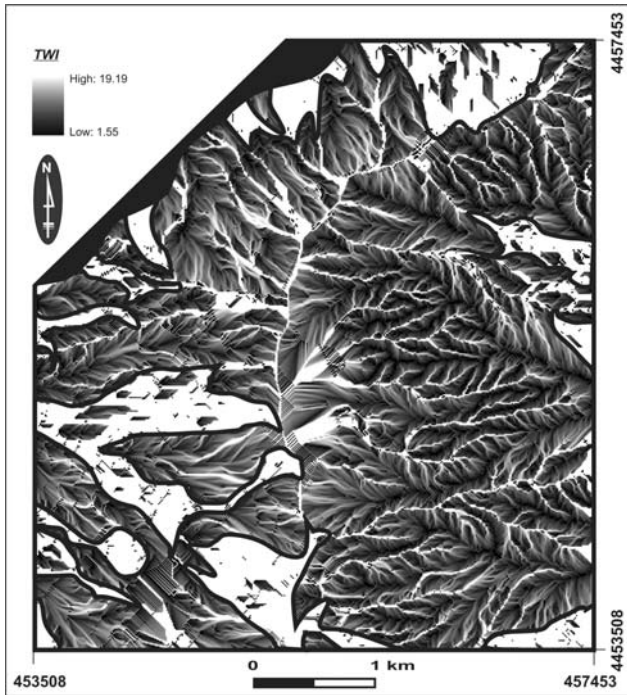


Fig. 9 Topographic wetness index (TWI) map and higher TWI values distributed in the higher elevations

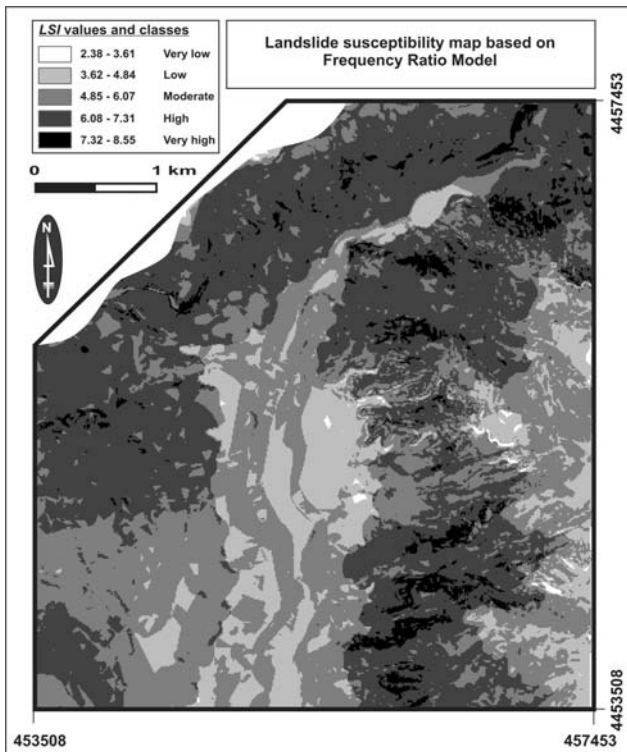


Fig. 10 Landslide susceptibility map based on frequency ratio

MAPping (SINMAP) (Pack et al. 1998a, b) was also made. This model requires three groups of input data (Fig. 12):

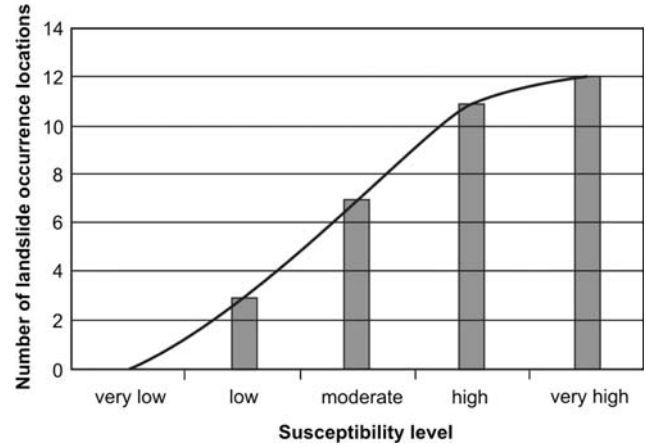


Fig. 11 Relationship between landslide occurrence locations with susceptibility map constructed from FR

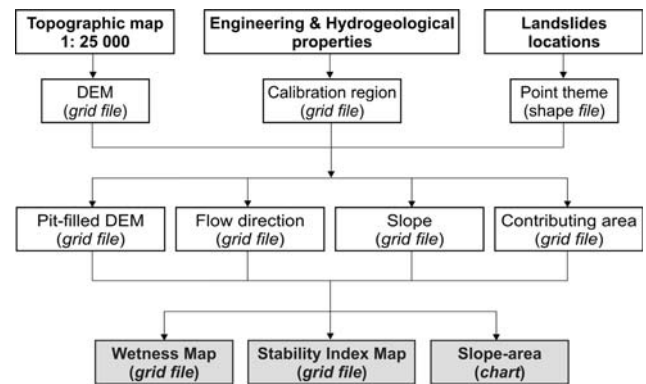


Fig. 12 The procedure of landslide susceptibility assessment based on SINMAP model

- terrain topography in a DEM grid format
- soil mechanical and hydraulic properties in a grid or polygon vector format
- landslide source areas inventory in a point vector format

For soil properties, the following data are required:

- range of cohesion values
- soil density value
- range of internal friction angle values
- range of recharge/transmissivity ratio

For calibration purposes a landslide inventory map is required; this was obtained from aerial or satellite orthophotos.

The output data are presented as:

- stability probability, expressed as a stability index divided into six classes
- TWI, divided into five classes

- graph of landslide occurrence with regard to slope and specific catchments area
- summary table

By adopting suitable ranges for variables it is possible to calibrate and group the majority of observed landslides into the smallest number of SI classes.

The SINMAP methodology is based upon the infinite slope stability model (e.g., Hammond et al. 1992) that balances the de-stabilizing components of gravity and the restraining components of friction and cohesion on a failure plane parallel to the ground surface; edge effects are neglected. It uses the “infinite slope” stability model formula for the factor of safety (FS) as discussed by, among many others, Hammond et al. (1992). The assumptions, mathematical manipulations and equations used in the model are presented in detail in the user manual of SINMAP (Pack et al. 1998a, b).

Parameters required by the SINMAP analysis were estimated based on in situ and laboratory tests. The map used showed that the geology of the region is homogenous; the volcanics were masked as they are not affected by any landslides. The following values were selected for the parameters input in the analysis:

- combined cohesion ( $c$ ): 0–0.45 kPa
- the internal friction angle of the soil ( $\Phi$ ): 5°–40°
- ratio recharge/transmissivity ( $R/T$ ): 500–2,500 (1/m)

In the first part of the SINMAP analyses, a number of secondary grids are defined, including: pit-filled DEM (pits are defined as grid elements that do not drain and hence are eliminated in the model), slope map, flow direction map and contributory area map. A grid is generated with a stability index (SI) at each grid cell location (Fig. 13). Table 4 shows the stability classes in terms of the stability index. The model also generates a slope–area plot (Fig. 14). A statistical summary by stability class is given in Table 5.

Six landslides in the study area were distributed in the stable zone of the susceptibility map and 27 landslides in the unstable zones (Table 5).

## Discussion and conclusions

In this paper, landslides in the study area were characterized by means of field and laboratory measurements, monitoring and remote sensing data. In order to predict future landslides in the area and its vicinity, landslide susceptibility maps were prepared using statistical (FR) and physical (SINMAP) data.

Field investigations, analysis of geological data and laboratory tests suggest that two important factors have acted together on this slope to cause sliding. The surface

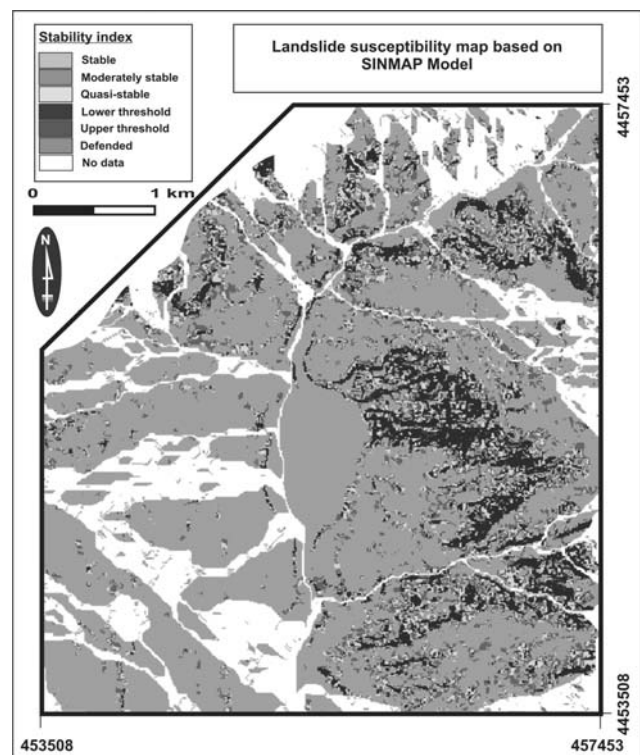


**Fig. 13** Landslide susceptibility map based on SINMAP model

water and groundwater circulation played an important role in initiating the movements while toe erosion is a predisposition factor. During heavy rainfall, water percolates into/through the Sebinkarahisar Formation, causing high pore water pressures and an increase in loading as the air voids are filled with water, resulting in a reduction in effective stress. Regressive upslope movement occurs following toe erosion and removal of the lateral support of the main upslope blocks. In addition, many of the slides occur where granular soils (sands and gravels) overlie permeable layers of silt and clay, or bedrock. Water seeping downward through the upper materials accumulates at the break of slope, forming a zone of weakness. Most slides occur during or after heavy rains (January through March) when the erosive capacity of the river is at its maximum and ground water levels are highest.

The FR model used such landslide-related factors as distance from the drainage system and roads, slope angle, slope aspect, TWI, topographical elevation and vegetation cover. The relationship between landslide occurrence locations and the susceptibility map showed that approximately 90% of the landslide occurrence locations fall into the susceptible classes. Validation indicated the high quality of susceptibility map.

Physically based landslide susceptibility mapping was carried out using the SINMAP model proposed by Pack et al. (1998a, b). It was found that 33% of all the

**Table 4** Stability classes in terms of the stability index (SI)

Condition	Class	Predicted state	Parameter range	Possible influence of factors not modeled
$SI > 1.5$	1	Stable slope zone	Range cannot model instability	Significant destabilizing factors are required for instability
$1.5 > SI > 1.25$	2	Moderately stable zone	Range cannot model instability	Moderate destabilizing factors are required for instability
$1.25 > SI > 1.0$	3	Quasi-stable slope zone	Range cannot model instability	Minor destabilizing factors could lead to instability
$1.0 > SI > 0.5$	4	Lower threshold slope zone	Pessimistic half of range required for instability	Destabilizing factors are not required for instability
$0.5 > SI > 0.0$	5	Upper threshold slope zone	Optimistic half of range required for stability	Stabilizing factors may be responsible for stability
$0.0 > SI$	6	Defended slope zone	Range cannot model stability	Stabilizing factors are required for stability

**Fig. 14** Slope area (SA) plot chart

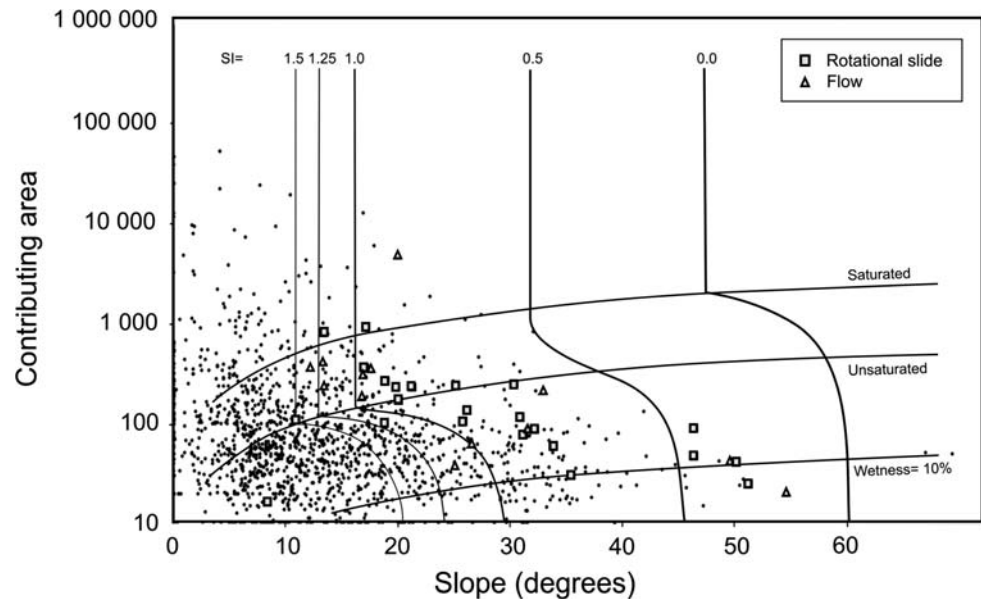


**Table 5** Statistical summary of stability classes for entire area

	Stable	Moderately stable	Quasi-stable	Lower threshold	Upper threshold	Defended	Total
Area (km <sup>2</sup> )	10.6	1.6	1.6	1.8	0.1	0.0	15.7
% of area	67.7	10.2	9.9	11.7	0.5	0.0	100
Landslides	1	2	3	21	6	0	33
% landslides	3.0	6.1	9.1	63.6	18.2	0.0	100
LS density	0.1	1.3	1.9	11.4	84.6	0.0	2.1

The terms of ‘lower threshold’ and ‘upper threshold’ are used to characterize regions where, according to the parameter uncertainty ranges quantified by the model, the probability of instability is less than or greater than 50% respectively. ‘Defended’ characterizes regions where, according to the model, the slope should be unstable for any parameters within the parameter ranges specified

landslides in the study area were located in the stable zone of the susceptibility map and 67% in the unstable zones.

The more realistic results were obtained from the FR model, probably because *SINMAP* is limited to shallow translational landslides, hence it is not really applicable for



deep-seated instability. It is likely that a susceptibility map produced by SINMAP would give more accurate results when used together with other terrain stability mapping methods, extensive field reconnaissance and the identification of homogenous zones with respect to soil properties.

Many methods of landslide remediation have been proposed, e.g., modification of slope geometry, drainage, retaining structures, internal slope reinforcement, etc. In the case of this particular study area, drainage alone will not stop the sliding as the movement is often initiated by removal of lateral support as a consequence of toe erosion and the loading of the hillside is immediate during heavy rainstorms which cannot be accommodated sufficiently quickly by drainage. As a consequence, in the study area the remedial measures must include retaining structures which should be designed to safeguard houses, roads, etc. Generally these are formed by reinforced concrete bored piles braced by reinforced concrete waling beams, which in the study area should be tied back into the andesite–basalts by ground anchors having a safe working load capacity. In addition, the toe erosion can be significantly reduced by the installation of bulkheads, such as large boulders at the edge of the creek. However, these will not resist significant lateral forces and indeed if a landslide occurs, material may pass over the bulkheads. Improvements in drainage and re-vegetation will also make an important contribution.

## References

- ArcGIS (version 9.1) (2005) Integrated geographical information system software. ESRI, CA
- ASTM (1990) Soil and rock; dimension stone; geosynthetics. American Society for testing and materials, Sect. 4, vol 04.08, designation: D421, D422, D4318
- Barka AA, Gülen L (1988) New constraints on age and total offset of the North Anatolian Fault Zone: implications for tectonics of the eastern Mediterranean region. *METU J Pure Appl Sci* 21(1–3):39–63
- Barredo JJ, Benavides A, Hervas J, Van Westen CJ (2000) Comparing heuristic landslide hazard assessment techniques using GIS in the Trijana basin, Gran Canaria Island, Spain. *JAG2* (1), pp 9–23
- Beven KJ, Kirkby MJ (1979) A physically based, variable contributing area model of basin hydrology. *Hydrol Sci Bull* 24:43–69
- Bonham-Carter GF (1994) *Geographic information systems for geoscientists, modeling with GIS*. Pergamon Press, Oxford, p 398
- Borga M, Dalla Fontana G, Da Ros D, Marchi L (1997) Shallow landslide hazard assessment using a physically based model and digital elevation data. *Environ Geol* 35(2/3):81–88
- Burt T, Butcher D (1986) Stimulation from simulation—a teaching model of hillslope hydrology for use on microcomputers. *J Geogr High Educ* 10:23–39
- Calcaterra D, de Riso R, Di Martire D (2004) Assessing shallow debris slide hazard in the Agnano Plain (Naples, Italy) using SINMAP, a physically based slope stability model. In: Lacerda WA, Ehrlich M, Fontoura SAB, Sayao ASF (eds) *Landslides: evaluation and stabilization*. Balkema. Taylor & Francis, London, pp 177–186
- Carrara A, Crosta G, Frattini P (2003) Geomorphological and historical data in assessing landslide hazard. *Earth Surf Processes Landf* 28:1125–1142
- Cascini L, Critelli S, Gulla G, Di Nocera S (1991) A methodological approach to landslide hazard assessment: a case history. In: *Proceedings of 16th international landslide conference*. Balkema, Rotterdam, pp 899–904
- Chacón J, Irigaray C, Fernández, T (1994) Large to middle scale landslide inventory, analysis and mapping with modelling and assessment of derived susceptibility, hazards and risks in a GIS. In: *Proceedings of 7th IAEG congress*, Balkema, Rotterdam, pp 4669–4678
- Chacón J, Irigaray C, Fernández T (1996) From the inventory to the risk analysis: Improvements to a large scale GIS method. In: Chacón J, Irigaray C, Fernández T (eds) *Proceedings of 8th international conference and field workshop on landslides*, Balkema, Rotterdam, pp 335–342
- Chacón J, Irigaray C, El Hamdouni R, Fernández T (2006) Engineering geology maps: landslides and geographical information systems. *Bull Eng Geol Environ* 65(4):341–411
- Chung CF, Fabbri AG (1999) Probabilistic prediction models for landslide hazard mapping. *Photogramm Eng Remote Sens* 65(12):1389–1399
- Dai FC, Lee CF, Zhang XH (2001) GIS-based geo-environmental evaluation for urban land-use planning: a case study. *Eng Geol* 61:257–271
- Dewey JF, Şengör AMC (1979) Aegean and surroundings regions: complex multiple and continuum tectonics in a convergent zone. *Geol Soc Am Bull* 90:84–92
- Ercanoğlu M, Gokceoglu C (2004) Use of fuzzy relations to produce landslide susceptibility map of a landslide prone area (West Black Sea Region, Turkey). *Eng Geol* 75:229–250
- Gokceoglu C, Aksoy H (1996) Landslide susceptibility mapping of the slopes in the residual soils of the Mengen region (Turkey) by deterministic stability analyses and image processing technique. *Eng Geol* 44:147–161
- Hall FG, Townshend JR, Engman ET (1995) Status of remote sensing algorithms for estimation of land surface state parameters. *Remote Sens Environ* 51:138–156
- Hammond C, Hall D, Miller S, Swetik P (1992) *Level I Stability Analysis (LISA) Documentation Version 2.0*, General Technical Report INT-285. United States Department of Agriculture, Forest Service Intermountain Research Station, USA
- Ives JD, Messerli B (1981) Mountain hazard mapping in Nepal: introduction to an applied mountain research project. *Mt Res Dev* 1(3–4):223–230
- Koçyiğit A (1989) Suşehri basin: an active fault-wedge basin on the North Anatolian Fault Zone, Turkey. *Tectonophysics* 167:13–29
- Koçyiğit A, Özacar AA (2003) Extensional neotectonic regime through the NE edge of the outer Isparta angle, SW Turkey: new field and seismic data. *Turkish J Earth Sci* 12:67–90
- Lee S, Min K (2001) Statistical analyses of landslide susceptibility at Yongin. *Korea Environ Geol* 40:1095–1113
- Lee S, Talib JA (2005) Probabilistic landslide susceptibility and factor effect analysis. *Environ Geol* 47:982–990
- McKenzie D (1972) Active tectonics of the Mediterranean region. *Geophys J R Astr Soc* 30:109–185
- Montgomery DR, Dietrich WE (1994) A physically based model for the topographic control on shallow landsliding. *Water Resour Res* 30(4):1153–1171
- Moore ID, Grayson RB, Ladson AR (1991) Digital terrain modeling—a review of hydro-hydrological, geomorphological, and biological applications. *Hydrol Processes* 5:3–30



- Pack RT, Tarboton DG, Goodwin CN (1998) A stability index approach to terrain stability hazard mapping. SINMAP user's manual, pp 68
- Pack RT, Tarboton DG, Goodwin CN (1998) Terrain stability mapping with SINMAP, technical description and users guide for version 1.00, report number 4114-0, Terratech Consulting Ltd., Salmon Arm ([www.tclbc.com](http://www.tclbc.com))
- Rodhe A, Seibert J (1999) Wetland occurrence in relation to topography: a test of topographic indices as moisture indicators. *Agric For Meteorol* 98–99:325–340
- Rupke J, Cammeraat E, Seijmonsbergen AC, Van Westen CJ (1988) Engineering geomorphology of the Widentobel catchment, Switzerland: a geomorphological inventory system applied to geotechnical appraisal of the slope stability. *Eng Geol* 26:33–68
- Seibert J, Bishop KH, Nyberg L (1997) A test of TOPMODEL's ability to predict spatially distributed groundwater levels. *Hydrol Processes* 11:1131–1144
- Şengör AMC (1980) Mesozoic–Cenozoic tectonic evolution of Anatolia and surrounding regions. Abstract, Bull Bur Rech Geol Minieres, France, pp 115–137
- Van Westen CJ (1993) Application of geographic information systems to landslide hazard zonation. Ph.D. dissertation Technical University Delft. ITC publication number 15, ITC, Enschede, p 245
- Van Westen CJ, Lulie Getahun F (2003) Analyzing the evolution of the Tessina landslide using aerial photographs and digital elevation models. *Geomorphology* 54(1–2):77–89
- Van Westen CJ, Soeters R, Sijmons K (2000) Digital geomorphological landslide hazard mapping of the Alpage area, Italy. *Int J Appl Earth Observ Geoinf* 2(1):51–59
- Varnes DJ (1978) Slope movement, types and processes. In: Schuster RL, Krizek RJ (eds) *Landslides, analyses and control*. National Academy of Science, report 176, Washington DC, pp 11–35
- Ward TJ, Ruh-Ming L, Simons DB (1982) Mapping landslide hazard in forest watershed. *J Geotech Eng Div, ASCE* 108(GT-2):319–324
- Weier J, Herring D (2005) Measuring vegetation (NDVI and EVI). Earth Observatory Library of NASA, <http://earthobservatory.nasa.gov/Library/MeasuringVegetation/>
- Yılmaz I (2007) GIS based susceptibility mapping of karst depression in gypsum: a case study from Sivas basin (Turkey). *Eng Geol* 90:89–103
- Yılmaz I, Yildirim M (2006) Structural and geomorphological aspects of the Kat landslides (Tokat-Turkey), and susceptibility mapping by means of GIS. *Environ Geol* 50(4):461–472
- Yılmaz A, Oral A, Bilgiç T (1985) Yukarı Kelkit çayı yöresi ve güneyinin temel jeoloji özellikleri ve sonuçları. M.T.A report (in Turkish)
- Zinko U, Seibert J, Dynesius M, Nilsson C (2005) Plant species numbers predicted by a topography based groundwater-flow index. *Ecosystems* 8:430–441